J Nanopart Res (2016) 18:64
DOI 10.1007/s11051-016-3374-5

RESEARCH PAPER

Synthesis of composite nanoparticles using co-precipitation of a magnetic iron-oxide shell onto core nanoparticles

Darinka Primc · Blaž Belec · Darko Makovec

Received: 16 July 2015 / Accepted: 18 February 2016 / Published online: 26 February 2016

Abstract Composite nanoparticles can be synthesized by coating a shell made of one material onto core nanoparticles made of another material. Here we report on a novel method for coating a magnetic iron oxide onto the surface of core nanoparticles in an aqueous suspension. The method is based on the heterogeneous nucleation of an initial product of Fe^{3+}/Fe^{2+} co-precipitation on the core nanoparticles. The close control of the supersaturation of the precipitating species required for an exclusively heterogeneous nucleation and the growth of the shell were achieved by immobilizing the reactive Fe^{3+} ions in a nitrate complex with urea ($[Fe((CO(NH_2)_2)_6](NO_3)_3$) and by using solid $Mg(OH)_2$ as the precipitating reagent. The slow thermal decomposition of the complex at 60 °C homogeneously releases the reactive Fe^{3+} ions into the suspension of the core nanoparticles. The key stage of the process is the thermal hydrolysis of the released Fe^{3+} ions prior to the addition of $Mg(OH)_2$. The thermal hydrolysis results in the formation of γ-FeOOH, exclusively at the surfaces of the core nanoparticles. After the addition of the solid hydroxide $Mg(OH)_2$, the pH increases and at pH ∼ 5.7 the Fe^{2+} precipitates and reacts with the γ-FeOOH to form magnetic iron oxide with a spinel structure (spinel ferrite) at the surfaces of the core nanoparticles. The proposed low-temperature method for the synthesis of composite nanoparticles is capable of forming well-defined interfaces between the two components, important for the coupling of the different properties. The procedure is environmentally friendly, inexpensive, and appropriate for scaling up to mass production.

Keywords Composite nanoparticles · Core–shell · Co-precipitation · Iron oxide · Maghemite · Magnetic nanoparticles · Colloids

Introduction

Composite nanoparticles showing multiple discrete functionalities integrated into a single nano-unit have recently been the subject of intense research because they could have widespread uses in advanced medical and other technological applications. While the properties of single-phase nanoparticles depend primarily on the intrinsic properties of the material they are made of, on their size and shape, the properties of composite nanoparticles can be modified on the basis

Electronic supplementary material The online version of this article (doi:10.1007/s11051-016-3374-5) contains supplementary material, which is available to authorized users.

D. Primc · B. Belec · D. Makovec (✉)
Department for Materials Synthesis, Jožef Stefan Institute and Jožef Stefan International Postgraduate School, Jamova cesta 39, 1000 Ljubljana, Slovenia
e-mail: Darko.Makovec@ijs.si

Present Address:
D. Primc
Laboratory for Multifunctional Materials, ETH Zürich, Vladimir-Prelog-Weg 5, 8093 Zurich, Switzerland

of interactions between the different properties in the materials being coupled. This coupling of the properties of different functional materials inside composite nanoparticles can lead to greatly improved or even completely new properties. In particular, composite nanoparticles combining two magnetically different materials (bi-magnetic nanoparticles) (Lopez-Ortega et al. 2015; Song and Zhang 2012; Estrader et al. 2013; Lee et al. 2011; Wang et al. 2010; Meffre et al. 2012; Primc and Makovec 2015) or synergetically combining a magnetic material with a material of another functionality, e.g., ferroelectric (Corral-Flores et al. 2010; Guduru et al. 2013), catalytic (Cheng et al. 2013; Zhou et al. 2010; Makovec et al. 2011), optical (Dosev et al. 2007; Wang et al. 2011), or plasmonic (Takahashi et al. 2015; Zhang et al. 2012), are especially interesting. In the vast majority of such multifunctional composite nanoparticles, the magnetic core is covered with a shell of another functional material. However, multifunctional core–shell nanoparticles can also be composed of a magnetic shell with cores of different materials, something that has seldom been reported. Typically, the reported methods involve the synthesis of spinel-ferrite shells with the thermal decomposition of organometallic compounds (e.g., metal acetylacetonate, metal–oleate complex, iron pentacarbonyl) in a high-boiling-point solvent (e.g., hexadecanediol, octadecene) (Song and Zhang 2012; Estrader et al. 2013; Lee et al. 2011; Wang et al. 2010; Meffre et al. 2012). The disadvantages of these methods are relatively high complexity and the need for expensive, frequently toxic, starting materials. All this makes scaling up the synthesis to an industrial level very difficult and raises environmental issues.

Composite nanoparticles composed of a magnetic shell at the core of a different material can also be synthesized using the simple co-precipitation of metal ions in an aqueous suspension of core nanoparticles (Primc and Makovec 2015). The magnetic iron-oxide shell can be formed by the heterogeneous nucleation and growth of the product of a simple co-precipitation of Fe^{2+}/Fe^{3+} ions at the surfaces of the core nanoparticles in their aqueous suspension. The process of co-precipitation has been extensively studied, as it is the basis for the method most frequently applied for the synthesis of magnetic iron-oxide nanoparticles (Massart 1981; Thanh 2012). These iron-oxide nanoparticles are applied in a variety of technologies, e.g., in ferrofluids (Blums et al. 1996), magnetic separation (Borlido et al. 2013), and medicine (Thanh 2012), for the detection, separation, or sorting of specific cells, for contrast enhancement in magnetic resonance imaging (MRI), for targeted drug delivery, and for cancer treatments using magnetically mediated hyperthermia, etc. The synthesis of magnetic nanoparticles with the co-precipitation of Fe^{2+}/Fe^{3+} ions from an aqueous solution involves homogeneous nucleation, which is the consequence of an uncontrolled, abrupt supersaturation of the precipitating species. The involved chemistry is actually quite complex and depends significantly on the experimental conditions, e.g., the reactant concentrations, the presence of counter ions, the temperature, etc. (Cornell and Schwertmann 2003). First, the Fe^{3+} precipitates even at a low pH of 2.8. Depending on the reaction conditions, the precipitated Fe(III) hydroxide transforms into iron-oxide hydroxide (FeOOH). If the FeOOH is in its γ-FeOOH structural modification (lepidocrocite), it will react with the Fe(II) hydroxide precipitating at a pH above $\sim$5.5 to form a magnetic spinel ferrite, initially magnetite (Fe_3O_4), which usually oxidizes to maghemite (γ-Fe_2O_3) when exposed to the ambient air. If the thermodynamically stable α-FeOOH (goethite) is formed after the precipitation of the Fe^{3+}, the magnetic phase will not be formed, as it can only transform to nonmagnetic hematite. Under acidic conditions, with a pH below 2.8, the Fe^{3+} ions can also slowly precipitate due to thermal hydrolysis at elevated temperatures (Cornell and Schwertmann 2003).

To form the shell on the core nanoparticles in the suspension, the precipitating species should heterogeneously nucleate and grow on the nanoparticle surfaces. Any precipitate that will nucleate homogeneously in the solution will result in the formation of a separate particle and not in deposition onto the core nanoparticle as a shell. To enable an exclusively heterogeneous nucleation during the precipitation, the supersaturation of the precipitating species should be carefully controlled. This supersaturation must be high enough for the heterogeneous nucleation to proceed, however, below the level required for a homogeneous nucleation. In general, the supersaturation is defined by the kinetics of the precipitation reactions and the reactant concentrations (Sugimoto 2001). Ionic chemical reactions in aqueous solutions, such as the precipitation of Fe ions, are generally very fast and

therefore difficult to control. To some extent, we can say that the supersaturation only depends on the concentrations of the reactants, which are very difficult to maintain homogeneously throughout the whole reaction mixture, even when the mixing is very intensive. An additional problem when controlling the supersaturation during the co-precipitation is in the difference of the pH value, where the two ions, i.e., Fe^{3+} (pH 2.8) and Fe^{2+} (pH $\sim$ 6), precipitate.

In our previous paper (Primc and Makovec 2015), we described the synthesis of bi-magnetic composite nanoparticles with a coating of soft-magnetic, spinel-ferrite, iron-oxide layers on a hard-magnetic, Ba-hexa-ferrite ($BaFe_{12}O_{19}$) platelet core. Direct, exchange-spring magnetic coupling between the hard-magnetic core and the soft-magnetic shell resulted in a large increase in the energy product $|BH|_{max}$, a figure of merit for the quality of magnets, by more than two times that of the core. This method can also be used for the synthesis of multifunctional composite nanoparticles by coating the spinel-ferrite iron-oxide shell on core nanoparticles of different functionalities. In this paper, we explain the chemistry that enables the synthesis of composite nanoparticles using the growth of the magnetic shell with the co-precipitation of the Fe^{2+}/Fe^{3+} ions onto the core nanoparticles in the aqueous suspension. To make the analysis of the product with transmission electron microscopy (TEM) easier, we used amorphous silica nanoparticles as the cores.

Experimental

Chemicals

Cabosil MP silica nanoparticles were purchased from Degussa Evonic, whereas the iron (III) nitrate hepta hydrate, iron (II) chloride, urea, magnesium hydroxide, and (3-Aminopropyl)triethoxysilane (98 %) were purchased from Alfa Aesar and used without further purification. A nitrate complex of Fe^{3+} with urea ($[Fe((CO(NH_2)_2)_6](NO_3)_3$), subsequently referred to as Fe^{3+}–urea, was synthesized according to the procedure described in the literature (Asuha et al. 2009). In brief, $Fe(NO_3)_3{\cdot}9H_2O$ (0.012 mol) was dissolved in ethanol (250 mL). Then, urea (0.1 mol) dissolved in 100 mL of ethanol was admixed into the Fe^{3+} ethanol solution. The complex formed as a green precipitate. After stirring the mixture at room temperature for 2 h, the precipitate was collected, washed with ethanol, and dried for subsequent reactions.

Preparation of aqueous suspensions of silica core nanoparticles

The suspension was prepared by suspending silica nanoparticles (0.8 mmol) in 50 mL of distilled water with ultrasound agitation (Sonics Vibra cell^{TM} ultrasonificator). The suspension remained stable due to the high, negative zeta potential of the silica (ζ-potential vs. pH; Figure SI1, Online Resource) that provides strong electrostatic repulsive forces between the nanoparticles. The globular nanoparticles had an average diameter of approximately 25 nm (TEM image; Figure SI2, Online Resource).

The suspension of the silica core nanoparticles with a positive surface charge was prepared by grafting hydrolyzed aminopropyl triethoxy silane (APS) onto their surfaces (Čampelj et al. 2009). The APS (0.1 mmol) was dissolved in ethanol (10 mL) and added into the aqueous suspension of the silica core nanoparticles (0.8 mmol, 50 mL), while the suspension was vigorously stirred. After the pH of the suspension was adjusted to 10.5 with diluted aqueous ammonia, it was heated for 6 h at 60 °C. After the reaction was completed, the silica core nanoparticles were washed with water and acetone to remove the unreacted hydrolyzed APS. The APS-grafted silica core nanoparticles were dispersed in distilled water, where the protonated amino groups of APS produced a high, positive surface charge below the isoelectric point at pH $\sim$ 9 (Figure SI1, Online Resource).

Synthesis of composite nanoparticles

The suspension of silica core nanoparticles (0.8 mmol, 50 mL) heated to a temperature of 60 °C was bubbled with argon to expel the dissolved oxygen. Then, a Fe^{3+}–urea complex ($n = 0.12$ mmol) and $FeCl_2$ ($n = 0.06$ mmol) were dissolved into the suspension, leading to an initial pH of 2.2. The amounts of reactants were calculated by assuming that a 3-nm-thick shell would form on the 25-nm-sized, globular core nanoparticles if all the Fe precursors would lead to the formation of the shell. After an incubation time t_1, ranging from 0 to 60 min, 0.24 mmol of $Mg(OH)_2$ was added to the reaction mixture, resulting in an

increase of the pH 2 h; after the addition of the $Mg(OH)_2$, the reaction mixture was cooled down. The whole procedure was performed under an inert argon atmosphere. Finally, the synthesized nanocomposite products were thoroughly washed with distilled water and dried in vacuum at room temperature for the analysis.

To obtain further insights into the mechanism of the spinel-ferrite formation, small volumes (approximately 5 mL) of the intermediate products were sampled during the early stages of the synthesis. The sampled suspensions were centrifuged immediately after sampling to separate the formed precipitates from the solution of the non-reacted precursors. The precipitates were washed with distilled water and re-suspended in the ethanol for the subsequent analyses. For measurements of the magnetic properties, the samples were dried in vacuum at room temperature. Table 1 lists the conditions used for the preparation of the individual samples. The names of the samples are composed of "S@Sil-*xx*-Sy," where "*xx*" denotes the incubation time t_1 and "Sy" denotes the stage of the process when the sample was extracted from the reaction mixture: S1—at the end of the first hydrolysis stage, S2—during the second stage, and S3—at the end of the deposition process (see text for details).

Characterization

The products were characterized using transmission electron microscopy (TEM) in combination with energy-dispersive X-ray spectroscopy (EDXS). For the TEM analysis, the composite nanoparticles were suspended in ethanol and deposited on a copper-grid-supported, perforated, electron-transparent carbon foil. A field-emission electron-source TEM JEOL 2010F equipped with an Oxford Instruments ISIS300 EDXS detector was operated at 200 kV. The EDXS spectra were quantified using Oxford ISIS software containing a library of virtual standards. The room-temperature magnetization M as a function of the magnetic field H of the dried samples was measured using a Lake Shore 7307 VSM vibrating-sample magnetometer. The zeta potentials of the suspended silica core nanoparticles were measured with electrokinetic measurements using a ZetaPALS Brookhaven Instruments Corporation Zeta-meter. In situ UV–Vis measurements were made using a Hewlett–Packard Model 8453 spectrometer.

Results and discussion

Thermal decomposition of the Fe^{3+}–urea complex

During the co-precipitation of the Fe^{2+}/Fe^{3+} ions from the aqueous solution, magnetic iron oxide is formed in the chain of chemical reactions and transformations (Cornell and Schwertmann 2003). We assumed that the final spinel-ferrite product remains as a coating at the core surfaces if the first solid phase that appears as a result of the precipitation (later referred to as the

Table 1 Conditions used for the synthesis of the samples, the detected phase after the precipitation of the Fe^{2+}/Fe^{3+} ions, and the type of nucleation

Sample	t_1 (min)	Sampling	Nucleation	Precipitated phase
S@Sil-10-S1	10	End of first stage	HEN	L
S@Sil-10-S2	10	Second stage	HEN	L, S
S@Sil-10-S3	10	Final sample	HEN	S
S@Sil-0-S2	0	Second stage	HEN, HON	S
S@Sil-0-S3	0	Final sample	HEN, HON	S
S@Sil-60-S1	60	End of first stage	HEN, HON	L, G
S@Sil-60-S2	60	Second stage	HEN, HON	L, G
S@Sil-60-S3	60	Final sample	HEN, HON	L, G
S@APS-Sil	10	Final sample	HEN	S

HON homogeneous nucleation in the solution, *HEN* heterogeneous nucleation at the surfaces of the core nanoparticles, *S* spinel ferrite (γ-Fe_2O_3), *L* lepidocrocite (γ-FeOOH), *G* goethite (α-FeOOH)

initial product) is heterogeneously nucleated at the core nanoparticles. The supersaturation needed for the heterogeneous nucleation of the initial product at the core nanoparticles is somewhat lower than that for the homogeneous nucleation in the solution. To favor heterogeneous nucleation of the initial product, its supersaturation should therefore be kept low and homogeneous throughout the whole reaction mixture. However, when the reactions are very fast, as in the case of the Fe^{2+}/Fe^{3+} precipitation, it is very difficult to maintain the homogeneity, even when intensive stirring is applied.

To ensure a low and homogeneous supersaturation, the reactive Fe^{3+} ions were immobilized into a nitrate complex with urea $[Fe((CO(NH_2)_2)_6](NO_3)_3$ (Fe^{3+}–urea complex). The Fe^{3+} ions were released from the complex in a controlled manner during its slow thermal decomposition. The non-homogeneity caused by the non-ideal mixing was reduced, since the Fe^{3+} ions were released homogeneously throughout the whole volume of the reaction mixture. We also assumed that the immobilization of the Fe^{3+} into a complex would postpone its precipitation to higher pH values, closer to that of the Fe^{2+} precipitation, enabling the simultaneous precipitation of the two ions.

Dissolving the Fe^{3+}–urea complex in water (1.5 mmol/L) resulted in a yellow solution of pH 2.2. At room temperature, the Fe^{3+}–urea complex remained stable, even when the pH was raised to the values above 10, which is well above the value of 2.8 required for the precipitation of the unbound Fe^{3+} ions. Only when the solution of the Fe^{3+}–urea complex (pH 2.2) was heated to temperatures above 48 °C did the color change from yellow to dark orange, indicating the thermal decomposition of the complex and the release of the Fe^{3+} ions. The complex's decomposition resulted in the release of Fe^{3+} ions, while the urea molecules most probably remained intact, since urea only starts to decompose at temperatures above 65 °C (Shaw and Bordeaux 1955). The released Fe^{3+} ions in the aqueous medium initially form the hexa-aqua ions $[Fe(H_2O)_6]^{3+}$, which at the elevated temperatures further hydrolyze to Fe oxide hydroxide (FeOOH) (Cornell and Schwertmann 2003). The process of the complex's decomposition can therefore be described with the following chemical reactions:

$$\left[Fe\left(CO(NH_2)_2\right)_6\right](NO_3)_3 \rightarrow Fe^{3+}(aq) + 3NO_3^-(aq) + 6(NH_2)_2CO$$

$$Fe^{3+}(aq) \rightarrow Fe(H_2O)_{6-n}^{(3-n)}(aq)$$

$$Fe(H_2O)_{6-n}^{3-n}(aq) \rightarrow FeOOH + 4 - nH_2O + 3H^+.$$

The thermal decomposition of the Fe^{3+}–urea complex at elevated temperatures was studied using in situ UV–Vis spectroscopy (Figure SI3, Online Resource). The results showed the start of the thermal decomposition at 48 °C, while at temperatures above 55 °C the FeOOH starts to form as a result of the thermal hydrolysis of the $[Fe(H_2O)_6]^{3+}$ ions. First, the formation of the γ-FeOOH phase was detected, whereas at higher temperatures and after longer times it partially transforms to the thermodynamically stable α-FeOOH phase.

Synthesis of the magnetic iron-oxide shell at the core nanoparticles

To deposit magnetic iron oxide onto the silica core surfaces, the initial product of the precipitation should nucleate exclusively heterogeneously at the core surfaces and, at the same time, the precipitation should proceed under conditions enabling the formation of the pure spinel-ferrite phase.

The process of deposition for the magnetic spinel ferrite onto the core nanoparticles can be divided into three stages. In the first stage, the stable aqueous suspension of core nanoparticles containing the iron precursors, i.e., the Fe^{3+}–urea complex and the Fe^{2+} ions, was maintained at elevated temperature for the incubation time needed for the decomposition of the Fe^{3+}–urea complex. Based on preliminary experiments, the optimal temperature for the complex's decomposition was determined to be 60 °C. After the incubation time, solid $Mg(OH)_2$ was admixed into the suspension. $Mg(OH)_2$ displays a relatively low solubility of 0.01 g/L (at 25 °C), which increases with the temperature (Greenwood and Earnshaw 2006). When the admixed $Mg(OH)_2$ was slowly dissolved, the hydroxyl ions were relatively homogeneously released into the reaction mixture, resulting in a gradual increase of the pH (Fig. 1). When the pH reaches a value of approximately 5.7, the Fe^{2+} ions start to

precipitate, marking the beginning of the second stage of the process. The third stage of the process begins when the final pH is reached. The reaction mixture was maintained at this final pH for 1.5 h.

The deposition process was analyzed by subtracting the samples after each stage (see Fig. 1) and analyzing them using TEM and magnetic measurements.

First stage of the deposition process

The color of the original suspension heated at 60 °C slowly changed from white to pale yellow-orange due to the decomposition of the Fe^{3+}–urea complex and the thermal hydrolysis of the released Fe^{3+} ions at the low pH of 2.2.

Figure 2a, b shows TEM images of the intermediate sample S@Sil-10-S1 retracted close to the end of the first stage (see Fig. 1). The images show that the surfaces of the silica cores are covered with small nanoparticles of approximately 3 nm. The nanoparticles were situated exclusively at the cores' surfaces in agreement with their formation via heterogeneous nucleation, while no separate, homogeneously nucleated particles were detected. EDXS analyses of the silica with the precipitate confirmed the formation of an Fe-rich phase (Figure SI4, Online Resource). Quantification of the spectra recorded over a large area of the material gave an average Fe/Si mass ratio of 0.10 ± 0.03. The electron diffraction (SAED) pattern taken from a larger area of the sample (Fig. 2c) shows a prevailing diffuse ring of amorphous silica and weak, sharper rings. During the thermal hydrolysis of the Fe^{3+} ions in the acidic aqueous medium, either γ-FeOOH or α-FeOOH is expected (Cornell and Schwertmann 2003; Fu et al. 2011; Navrotsky et al. 2008). The recorded SAED pattern matched with the calculated pattern for the orthorhombic phase of γ-FeOOH (Fig. 2c). The formation of γ-FeOOH with the thermal hydrolysis of the Fe^{3+} released from the complex is also in accordance with UV–Vis spectroscopy (see Online Resource). Due to the presence of FeOOH nanoparticles on the surfaces of the diamagnetic silica, the sample S@Sil-10-S1 displayed weak paramagnetic properties (Fig. 3).

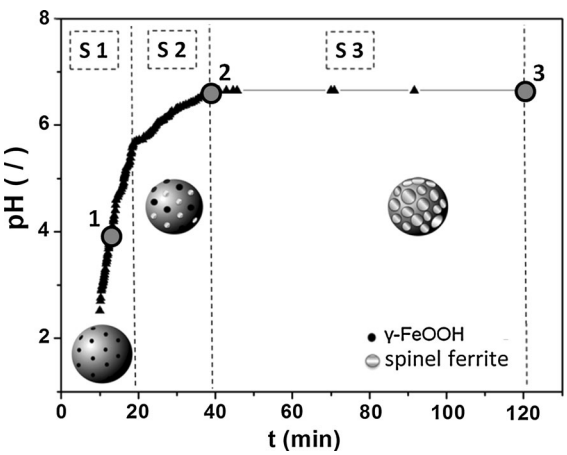

Fig. 1 pH versus time curve measured during the synthesis of the S@Sil-10 samples (S1, S2, and S3 mark three stages of the process, *circles* marked with 1, 2, and 3 show the subtraction time of the samples S@Sil-10-S1, S@Sil-10-S2, and S@Sil-10-S3, respectively)

Second stage of the deposition process

The first, hydrolysis stage of the process ends after the addition of $Mg(OH)_2$ gives rise to an increase in the pH resulting in the precipitation of Fe^{2+}. At that point in the process, the color of the suspension turns brownish. The length of time allowed for the thermal hydrolysis (the incubation time t_1) influences the initial slope of the pH versus time curve and the final pH reached. In the case of a t_1 of 10 min, a pH of 5.7, required for the Fe^{2+} precipitation, was obtained within 9 min after the addition of the $Mg(OH)_2$ (Fig. 1). As the hydroxyl ions released with the dissolution of $Mg(OH)_2$ are consumed for the precipitation reaction, the slope of the curve decreased (Fig. 1), marking the beginning of the second stage. The second stage finishes after another 10 min, when a final pH of 6.8 was reached (Fig. 1). Figure 2d shows a representative TEM image of the sample S@Sil-10-S2 extracted from the mixture immediately after the pH reached 5.7 (Fig. 1). The size and the surface concentration of the small nanoparticles on the silica increased. Quantification of the EDXS spectra recorded over a large area of the material gave an average Fe/Si mass ratio of 0.20 ± 0.05. A detailed TEM examination revealed the absence of any homogeneously nucleated nanoparticles. The nanoparticles' size increased from approximately 3 nm after the first stage (sample S@Sil-10-S1), to approximately 5 nm in the sample S@Sil-10-S2, and with the increased size, the crystalline order also improved (Fig. 2e). The periodicity of the lattice fringes marked in the image of the nanoparticle in Fig. 2e corresponds to the (111)

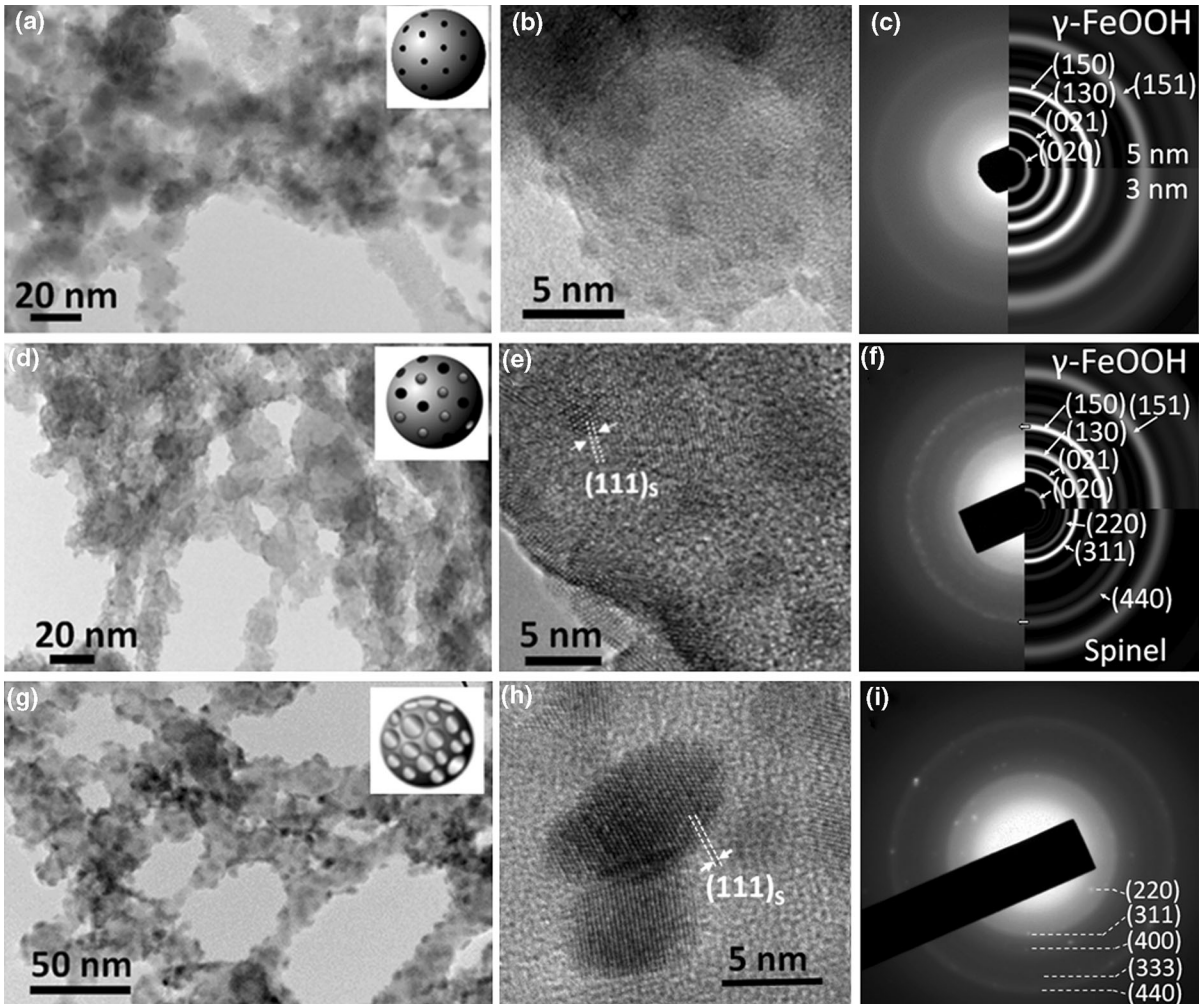

Fig. 2 Representative TEM images, HRTEM images, and the corresponding electron diffraction patterns of the samples extracted from the reaction mixture after different stages of the deposition process: (**a–c**) sample S@Sil-10-S1 extracted at the end of the first stage (the experimental SAED pattern is compared with the calculated ones for the γ-FeOOH structure with nanoparticle sizes of 5 nm (*top right*) and 3 nm (*bottom right*)), (**d–f**) sample S@Sil-10-S2 extracted during the second stage (the experimental SAED pattern is compared with the calculated ones for the 5-nm nanoparticles of the cubic spinel structure (*bottom right*) and the 5-nm nanoparticles of the orthorhombic γ-FeOOH structure (*top right*)), and (**g–i**) final sample S@Sil-10-S3 (the SAED pattern is indexed according to the spinel structure)

interplanar distances of the spinel structure. The corresponding SAED pattern (Fig. 2e) reveals reflection rings that can be ascribed to two phases: spinel ferrite and γ-FeOOH.

The *M* versus *H* curve for the sample S@Sil-10-S2 shows a weak superparamagnetic behavior. The deviation from a linear, paramagnetic curve is very small because of the small amount of spinel-ferrite nanoparticles. The slope of the linear part of the curve (susceptibility) at high *H* is larger than that of the sample extracted after the first stage (sample S@Sil-10-S1), because of a larger content of the deposited iron species.

The results clearly show that spinel ferrite forms as part of the reaction of the precipitating Fe^{2+} ions with the γ-FeOOH formed during the thermal hydrolysis at the surfaces of the core nanoparticles. In general, the γ-FeOOH-to-spinel ferrite transformation can proceed along different pathways. The transformation proceeds either with the dissolution–recrystallization process at pH values below 4 and above 10, or with in situ dehydration and a local structural rearrangement at pH

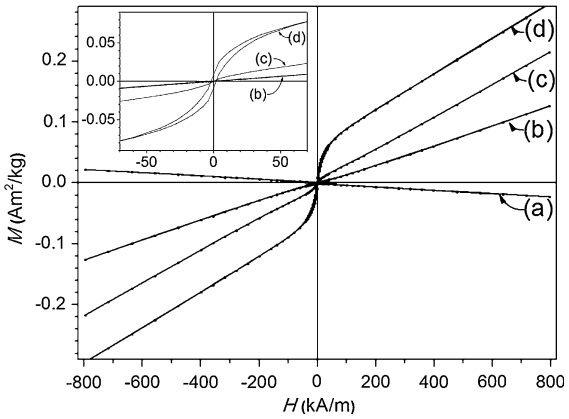

Fig. 3 Magnetization *M* versus magnetic field *H* for silica core nanoparticles (**a**) and samples extracted from the reaction mixture after the first stage (**b**), after the second stage (**c**), and at the end (**d**) of the deposition process. The diamagnetic contribution of the silica was subtracted from the magnetizations of the samples

values between 4 and 10 (Cudennec and Lecerf 2005; Jolivet et al. 2004). The solid transformation with a structural rearrangement is initiated with the adsorption of Fe^{2+} on the γ-FeOOH surfaces. Since in our experiments the Fe^{2+} ions precipitated close to the neutral pH, it can be concluded that the γ-FeOOH-to-spinel transformation proceeds with the dehydration and the local structural rearrangement initiated by the precipitated Fe^{2+}. The described mechanism is also favorable in terms of retaining the final spinel-ferrite product as the coating on the core nanoparticles after the transformation from γ-FeOOH.

Third stage of the deposition process

In the third, final stage of the deposition process, the γ-FeOOH-to-spinel transformation is completed. TEM analyses of the final sample S@Sil-S3 (Fig. 2g, h) show that the nanoparticles on the surfaces of the silica core nanoparticles grow to 5–7 nm in size during the final stage of the process. The EDXS analyses showed the average composition with an Fe/Si mass ratio of 0.23 ± 0.05. The corresponding SAED pattern matches with the cubic spinel structure (Fig. 2i). Taking into consideration the experimental conditions used during the synthesis under an inert atmosphere, the first spinel-ferrite phase formed is most likely magnetite (Fe_3O_4). However, the small magnetite nanoparticles are prone to oxidation into maghemite (γ-Fe_2O_3) when exposed to the ambient air.

Due to the transformation of all the FeOOH into the magnetic spinel ferrite and due to the growth of the spinel-ferrite nanoparticles, the ferrimagnetic contribution to the *M* versus *H* curve for the sample S@Sil-10-S3 is larger than that for the sample S@Sil-10-S2 (Fig. 3). Also, the susceptibility at high *H* (linear part of the curve) was somewhat larger than that for the sample S@Sil-10-S2, because of the small increase in the content of the iron ions.

Influence of the duration of the thermal hydrolysis stage on the final product

An analysis of the deposition process showed that the nanoparticles of the γ-FeOOH precipitate with the thermal hydrolysis at low pH even before the addition of $Mg(OH)_2$. The effect of the thermal hydrolysis on the appearance of the final product was studied by examining the samples synthesized without the thermal hydrolysis stage ($t_1 = 0$) and by maintaining the reaction suspension at 60 °C for a long incubation time t_1 of 60 min (Table 1).

The synthesis under the reaction conditions where the thermal hydrolysis was almost absent was conducted by the addition of $Mg(OH)_2$ into the suspension of the silica cores together with the Fe precursors (sample S@Sil-0-S3). As is evident from the pH vs. time curve (Fig. 4a), the increase in the pH of the suspension was much steeper than that measured during the synthesis of the S@Sil-10-S3 sample, where the $Mg(OH)_2$ was admixed after 10 min. The pH reached a value of 5.7 after 3 min, and it further increased to a value of 8 after another 3 min. The intermediate product S@Sil-0-S2 sampled immediately after the pH reached a value of 5.7 and consisted of two types of particles: the larger amorphous silica core nanoparticles, covered with smaller crystalline nanoparticles, and the agglomerates of smaller spherical crystalline nanoparticles, 3–5 nm in size (Fig. 4b). The EDXS analysis confirmed the formation of the Fe-rich phase, while the SAED pattern (Fig. 4c) showed weak diffraction rings that can be indexed according to the spinel structure. A detailed TEM observation revealed the absence of other Fe phases. Obviously, the agglomerated spinel nanoparticles lying separately from the silica cores (marked with arrows in Fig. 4b) were nucleated homogeneously in the solution. The rapid increase in the concentration of the hydroxyl ions increased the supersaturation of the

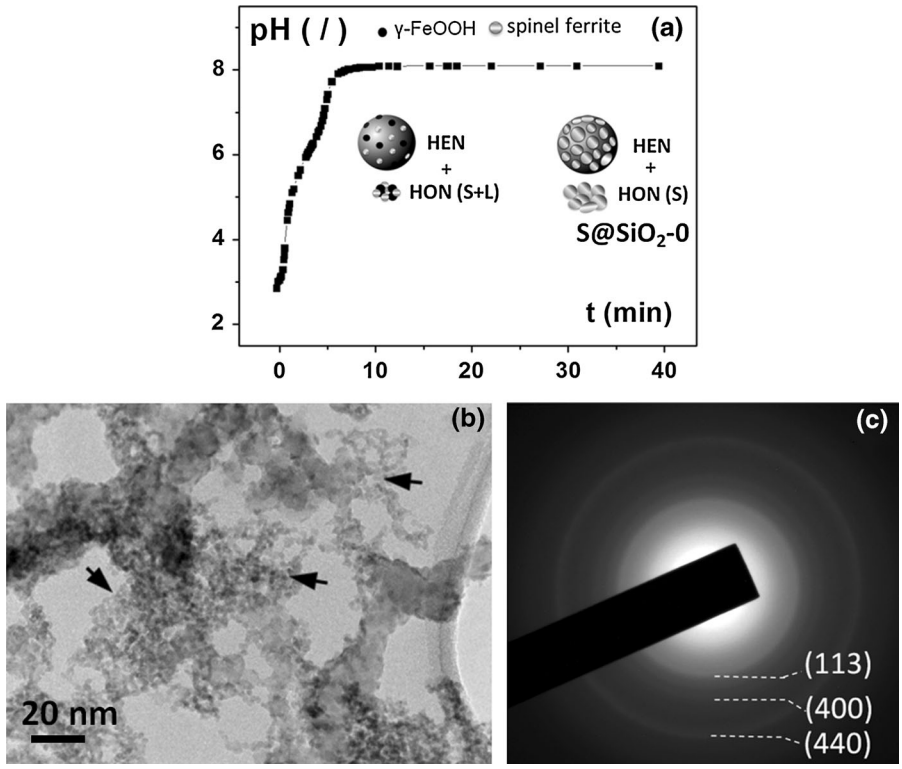

Fig. 4 **a** pH versus time curve measured during the synthesis of the S@Sil-0 sample (*HEN* heterogeneous nucleation, *HON* homogeneous nucleation), **b** representative TEM image of S@Sil-0-S2 sample, and **c** the corresponding electron diffraction pattern indexed according to a spinel structure

initial product to above the value required for homogeneous nucleation.

Also in the case when the first stage of the synthesis was long, allowing a long time for the decomposition of the complex and for the thermal hydrolysis of the released Fe^{3+} ions, the pH increased sharply after the addition of the $Mg(OH)_2$. During the synthesis of the S@Sil-60-S3 sample ($t_1 = 60$ min), the pH of 5.8 required for the Fe^{2+} precipitation was reached in 3 min, while the final pH of 7.2 was reached in another 10 min (Fig. 5a). Figure 5b shows a TEM image of the intermediate sample S@Sil-60-S1 extracted at the end of the first stage. The TEM revealed that the surfaces of the silica core nanoparticles were partially covered with small nanoparticles of sizes between 3 and 5 nm. The electron diffraction pattern recorded from the large area reveals the diffuse rings that can be ascribed to the α-FeOOH structure; however, the two rings can also be ascribed to the γ-FeOOH structure. Separate, homogeneously nucleated FeOOH nanoparticles were never observed in the sample. The formation of both phases is consistent with the employed reaction conditions (Cornell and Schwertmann 2003; Fu et al. 2011; Navrotsky et al. 2008) and with our study of the thermal decomposition of the Fe^{3+}–urea complex (see Online Resource).

The TEM of the intermediate sample S@Sil-60-S2, extracted after the addition of $Mg(OH)_2$, which increased the pH of the reaction mixture to a value of 5.7, showed the presence of larger, sheet-like particles (marked with arrows in Fig. 5d) in addition to the silica core nanoparticles covered with the small nanoparticles of approximately 3–5 nm (Fig. 5e). The corresponding SAED pattern (Fig. 5f) indicated the presence of two different phases: the diffraction rings originating from the nanoparticles at the surfaces of the cores match to the spinel structure, while the discrete reflections originating from separate sheet-like particles match to the γ-FeOOH structure. The detailed TEM observations revealed that all the spinel-ferrite nanoparticles are located exclusively at the surfaces of the silica cores.

The TEM of the final S@Sil-60-S3 sample (Fig. 5g) revealed that apart from the silica core nanoparticles covered with the spinel nanoparticles, large rod-like particles, approximately 300 nm long and 50 nm thick, were present. The size of the spinel nanoparticles located at the silica cores increased to

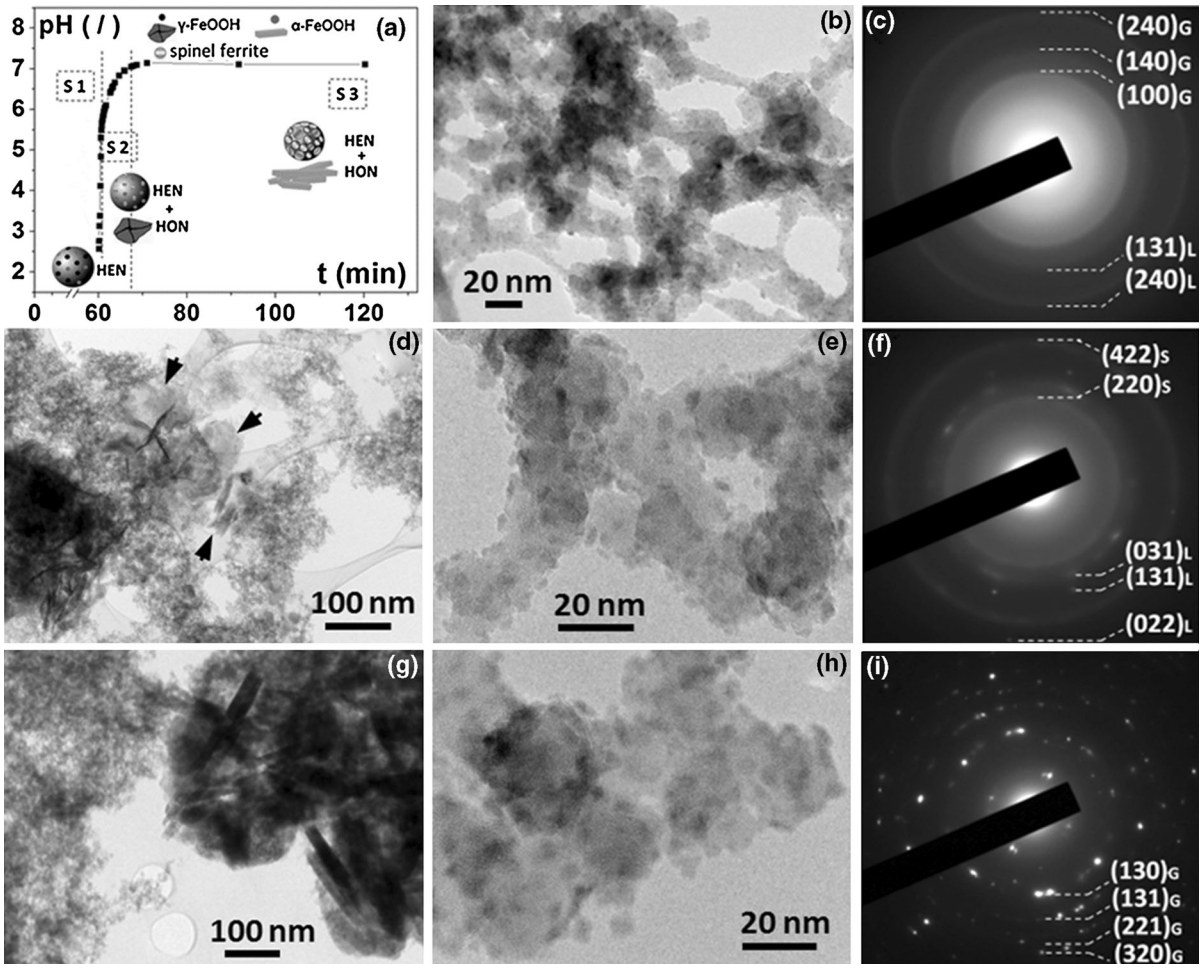

Fig. 5 **a** pH versus time curve measured during the synthesis of the S@Sil-60 samples (S1, S2, and S3 mark three stages of the process, *HEN* heterogeneous nucleation, *HON* homogeneous nucleation), **b** representative TEM image of the S@Sil-60-S1 sample, **c** corresponding electron diffraction pattern indexed according to the γ-FeOOH structure (L) and the α-FeOOH structure (G), **d** and **e** representative TEM images of the S@Sil-60-S sample, **f** corresponding electron diffraction pattern indexed according to the γ-FeOOH structure (L) and the spinel structure (S), **g** and **h** representative TEM images of the final S@Sil-60-S3 sample, and **i** corresponding electron diffraction pattern indexed according to the α-FeOOH structure (G)

5 nm (Fig. 5h). The SAED pattern (Fig. 5i) recorded for the area with the rod-like particles reveals a well-crystallized phase with discrete reflections that can be indexed according to the α-FeOOH structure.

The examination of the intermediate sample S@Sil-60-S1 revealed that the γ-FeOOH nanoparticles, formed at the core surfaces through heterogeneous nucleation during a prolonged thermal hydrolysis, partially transformed to the α-FeOOH phase. The transformation between the two FeOOH modifications is influenced by the size of the formed nanoparticles, which depends on the concentration of the Fe^{3+} ions, temperature, and time. The γ-FeOOH phase forms initially as smaller nanoparticles, with sizes below approximately 5 nm. However, as the γ-FeOOH nanoparticles grow, they transform to the thermodynamically stable α-FeOOH phase. The lower formation enthalpy makes the α-FeOOH phase more stable in comparison to the γ-FeOOH phase. However, for very small nanoparticles, the hydration enthalpy becomes an important parameter, making γ-FeOOH the stable phase due to the increased surface-to-volume ratio (Fu et al. 2011; Navrotsky et al. 2008). The α-FeOOH phase formed after the prolonged thermal hydrolysis step does not react with the Fe^{2+} precipitated after the addition of $Mg(OH)_2$ to form the

magnetic spinel ferrite. Instead, the precipitation of Fe^{2+} results in the formation of the sheet-like particles of the γ-FeOOH phase. During aging at 60 °C, these sheet-like particles transform into the rod-like particles of α-FeOOH present in the final S@Sil-60-S3 sample.

Influence of the surface charge of the core nanoparticles on the coating

To evaluate the influence of the surface charge of the core nanoparticles on the heterogeneous nucleation of the product, the synthesis was also performed in a colloidal suspension of positively charged silica nanoparticles APS-Sil. This experiment is also important to exclude the possibility that the spinel nanoparticles were formed after homogeneous nucleation in the solution and subsequently adhered to the silica nanoparticle surfaces only due to the electrostatic attractions. The iron-oxide nanoparticles display a positive surface charge in the acidic aqueous suspension, whereas the pristine silica nanoparticles used as the cores in the synthesis exhibited a highly negative zeta potential across the whole pH region where the reaction proceeds (pH 2–7) (see Figure SI1, Online Resource) (Čampelj et al. 2009). Thus, the formed iron-oxide nanoparticles and the silica core nanoparticles would be oppositely charged and might fuse together due to the electrostatic attractions. However, when the sample (S@APS-Sil) was synthesized using the positively charged, APS-grafted, silica core nanoparticles, its appearance was not significantly different (see Figure SI5, Online Resource) from the sample S@Sil-10 prepared with the pristine, negatively charged silica cores. The charge at the cores' surfaces had no noticeable influence on the nucleation. The experiment proves that the spinel-ferrite nanoparticles really deposit onto the cores after the heterogeneous nucleation of the precipitating species at the surfaces of the silica cores.

Final discussion

We demonstrated the chemistry behind a new method that can be used for the synthesis of composite nanoparticles combining a core nanoparticle of different functional materials with a magnetic shell. The method is based on coating the magnetic spinel-ferrite shell onto the core nanoparticles with the co-precipitation of Fe^{3+}/Fe^{2+} in the aqueous suspension. The key is in the close control of the supersaturation of the precipitating species resulting in an exclusively heterogeneous nucleation and growth of the magnetic shell, which was achieved by the controlled release of the reactive Fe^{3+} ions with the thermal decomposition of an Fe^{3+}–urea complex. The synthesis is conducted in aqueous media, using simple raw materials; it is also environmentally friendly, inexpensive, and appropriate for scaling up to mass production.

The method could be especially important for the synthesis of new composites, where the functional properties of the two components are coupled. As the coating of the magnetic shell onto the core nanoparticles is conducted at a relatively low temperature (60 °C), no chemical reactions or the inter-diffusion of atoms between the two components are expected. It was shown (Juhin et al. 2014) that the inter-diffusion between the two components of the composite nanoparticles severely diminishes the coupling. This inter-diffusion is a large problem in composite nanoparticles synthesized by the thermal decomposition of organometallic compounds conducted at temperatures close to 300 °C (Juhin et al. 2014).

With some adaptations, the method can also be applied for the synthesis of a shell made of other spinel ferrites, when Fe^{2+} is exchanged with other two-valent metal ions, e.g., Zn^{2+}, Co^{2+}, Mn^{2+}, Ni^{2+}, etc.

Conclusions

The coating of a magnetic spinel-ferrite iron-oxide shell onto core nanoparticles was studied as a method for synthesizing new, multifunctional, composite nanoparticles. The shell forms with the heterogeneous nucleation and growth of the product of the co-precipitation of Fe^{3+}/Fe^{2+} ions in an aqueous suspension of core nanoparticles. The low and homogeneous supersaturation required for the exclusively heterogeneous nucleation of an initial product during the precipitation of the Fe^{3+} ions was enabled by the slow thermal decomposition of an Fe^{3+}–urea nitrate complex ($[Fe((CO(NH_2)_2)_6](NO_3)_3$). First, the suspension of the core nanoparticles containing the dissolved complex and the Fe^{2+} ions (pH $\sim$ 2.2) is maintained at elevated temperature (60 °C). The reactive Fe^{3+} ions released from the complex slowly hydrolyze and γ-FeOOH is formed exclusively on the surfaces of the

core nanoparticles. After the addition of solid hydroxide $Mg(OH)_2$, the pH increases, and at pH $\sim$ 5.7 the Fe^{2+} precipitates. The precipitated Fe^{2+} reacts with the γ-FeOOH on the surfaces of the core nanoparticles to form a magnetic spinel ferrite. If the thermal hydrolysis step is omitted, a part of the γ-FeOOH nucleates homogeneously, forming separate nanoparticles. When the time allowed for the thermal hydrolysis is too long, the γ-FeOOH at the surfaces of the core nanoparticles partially transforms into thermodynamically stable α-FeOOH, which does not further transform into the magnetic spinel ferrite.

As it proceeds at a relatively low temperature, the proposed method for the synthesis of the composite nanoparticles is capable of forming well-defined interfaces between the two components, important for the coupling between different properties. It is environmentally friendly, inexpensive, and appropriate for scaling up to mass production.

Acknowledgments The support of the Ministry of Higher Education, Science and Technology of the Republic of Slovenia within National Research Program P2-0089 is gratefully acknowledged. The authors also acknowledge the use of equipment in the Center of Excellence on Nanoscience and Nanotechnology – Nanocenter.

References

Asuha S, Zhao S, Jin XM, Hai MM, Bao HP (2009) Effects of synthetic routes of Fe–urea complex on the synthesis of γ-Fe_2O_3 nanopowder. Appl Surf Sci 255:8897–8901

Blums A, Cebers M, Maiorov M (1996) Magnetic fluids. Walter de Gruyter & Co., Berlin

Borlido L, Azevedo AM, Roque ACA, Aires-Barros MR (2013) Magnetic separations in biotechnology. Biotech Adv 31:1374–1385

Čampelj S, Makovec D, Drofenik M (2009) The functionalization of magnetic nanoparticles with 3-aminopropyl silane. J Mag Mag Mat 321:1346–1350

Cheng M, Xie W, Zong B, Sun B, Qiao M (2013) When magnetic catalyst meets magnetic reactor: etherification of FCC light gasoline as an example. Nat Commun 3:19731–19735

Cornell RM, Schwertmann U (2003) The iron oxides, structure, properties, reactions, occurrences and uses. Wiley-VCH, Weinheim

Corral-Flores V, Bueno-Baques D, Ziolo R (2010) Synthesis and characterization of novel $CoFe_2O_4$-$BaTiO_3$ multiferroic core–shell-type nanostructures. Acta Mater 58:764–769

Cudennec Y, Lecerf A (2005) Topotactic transformation of goethite and lepidocrocite into hematite and maghemite. Sol State Sci 7:520–529

Dosev D, Nichkova M, Dumas RK, Gee SJ, Hammock BD, Liu K, Kennedy IM (2007) Magnetic/luminescent core/shell particles synthesized by spray pyrolysis and their application in immunoassays with internal standard. Nanotechnology 18:055102–055112

Estrader M, Lopez-Ortega A, Estrade S, Golosovsky IV, Salazar-Alvarez G, Vasilakaki M, Trohidou KN, Varela M, Stanley DC, Sinko M, Pechan MJ, Keavney DJ, Peiro F, Surinach S, Baro MD, Nogues J (2013) Robust antiferromagnetic coupling in hard-soft Bi-magnetic core/shell nanoparticles. Nat Commun 4:2960–2967

Fu D, Keech PG, Sun X, Wren CJ (2011) Iron oxyhydroxide nanoparticles formed by forced hydrolysis: dependence of phase composition on solution concentration. Phys Chem Chem Phys 13:18523–18529

Greenwood NN, Earnshaw A (2006) Chemistry of elements. Elsevier Butterworth-Heinemann, Oxford

Guduru R, Liang P, Runowicz C, Nair M, Atluri V, Khizroev S (2013) Magneto-electric nanoparticles to enable field-controlled high-specificity drug delivery to eradicate ovarian cancer cells. Sci Rep 3:29531–29538

Jolivet JP, Chaneac C, Tronc E (2004) Iron oxide chemistry. From molecular clusters to extend solid networks. Chem Commun 20:481–487

Juhin A, Lopez-Ortega A, Sikora M, Carvallo C, Estrader M, Estrade S, Peiro F, Dolors Baro M, Sainctavit P, Glatzeli P, Nogues J (2014) Direct evidence for an interdiffused intermediate layer in Bi-magnetic core-shell nanoparticles. Nanoscale 6:11911–11920

Lee J-H, Jang J-T, Choi J-S, Moon S-H, Noh S-H, Kim J-W, Kim J-G, Kim I-S, Park K-I, Cheon J (2011) Exchange-coupled magnetic nanoparticles for efficient heat induction. Nat Nanotechnol 6:418–422

Lopez-Ortega A, Estrader M, Salazar-Alvarez G, Roca AG, Nogues J (2015) Applications of exchange coupled Bi-magnetic hard/soft and soft/hard magnetic core/shell nanoparticles. Phys Rep 553:1–32

Makovec D, Sajko M, Selišnik A, Drofenik M (2011) Magnetically recoverable photocatalytic nanocomposite particles for water treatment. Mater Chem Phys 129:83–89

Massart R (1981) Preparation of aqueous magnetic liquids in alkaline and acidic media. IEEE Trans Magn 17:1247–1248

Meffre A, Mehdaoui B, Kelsen V, Fazzini PF, Carrey J (2012) A simple chemical route toward monodisperse iron carbide nanoparticles displaying tunable magnetic and unprecedented hyperthermia properties. Nano Lett 12:4722–4728

Navrotsky A, Mazeina L, Majzlan J (2008) Size-driven structural and thermodynamic complexity in iron oxides. Science 319:1635–1638

Primc D, Makovec D (2015) Composite nanoplatelets combining soft-magnetic iron oxide with hard-magnetic barium hexaferrite. Nanoscale 7:2688–2697

Shaw WR, Bordeaux JJ (1955) The decomposition of urea in aqueous media. J Am Chem Soc 77:4729–4733

Song Q, Zhang ZJ (2012) Controlled synthesis and magnetic properties of bimagnetic spinel ferrite $CoFe_2O_4$ and $MnFe_2O_4$ nanocrystals with core–shell architecture. J Am Chem Soc 134:10182–10190

Sugimoto T (2001) Monodispersed particles. Elsevier, Amsterdam

Takahashi M, Mohan M, Nakade A, Higashimine K, Mott D, Hamada T, Matsumura K, Taguchi T, Maenosono S (2015)

Ag/FeCo/Ag core/shell/shell magnetic nanoparticles with plasmonic imaging capability. Langmuir 31:2228–2236

Thanh TKN (ed) (2012) Magnetic nanoparticles: from fabrication to clinical applications. CRC Press, Boca Raton

Wang L, Wang X, Luo J, Wanjala BN, Wang C, Chernova NA, Engelhard MH, Liu Y, Bae I-T, Zhong C-J (2010) Core-shell-structured magnetic ternary nanocubes. J Am Chem Soc 132:17686–17689

Wang H, Sun L, Li Y, Fei X, Sun M, Zhang C, Li Y, Yang Y (2011) Layer-by-layer assembled Fe_3O_4@C@CdTe core/shell microspheres as separable luminescent probe for sensitive sensing of Cu^{2+} ions. Langmuir 27:11609–11615

Zhang H, Harpster MH, Wilson WC, Johnson PA (2012) Surface-enhanced raman scattering detection of DNAs derived from virus genomes using Au-coated paramagnetic nanoparticles. Langmuir 28:4030–4037

Zhou L, Gao Z, Xu W (2010) Robust Fe_3O_4/SiO_2-Pt/Au/Pd magnetic nanocatalysts with multifunctional hyperbranched polyglycerol amplifiers. Langmuir 26:11217–11225